J|A|C|S ARTICLES

Published on Web 10/25/2010

# The Conformational Free-Energy Landscape of β-D-Mannopyranose: Evidence for a $^1S_5 \rightarrow B_{2,5} \rightarrow {}^OS_2$ Catalytic Itinerary in β-Mannosidases

Albert Ardèvol,[†] Xevi Biarnés,[‡] Antoni Planas,[‡] and Carme Rovira*[,†,§]

*Computer Simulation and Modeling Laboratory and Institut de Química Teòrica i Computacional (IQTCUB), Parc Científic de Barcelona, Baldiri Reixac 10-12, 08028 Barcelona, Spain, Laboratory of Biochemistry, Institut Químic de Sarrià, Universitat Ramon Llull, Via Augusta 390, 08017 Barcelona, Spain, and Institució Catalana de Recerca i Estudis Avançats (ICREA), Passeig Lluís Companys 23, 08018 Barcelona, Spain*

Received June 23, 2010; E-mail: crovira@pcb.ub.es

***Abstract:*** The mechanism of glycosidic bond cleavage by glycosidases involves substrate ring distortions in the Michaelis complex that favor catalysis. Retaining β-mannosidases bind the substrate in a $^1S_5$ conformation, and recent experiments have proposed an unusual substrate conformational pathway ($^1S_5 \rightarrow B_{2,5} \rightarrow {}^OS_2$) for the hydrolysis reaction. By means of Car−Parrinello metadynamics simulations, we have obtained the conformational free-energy surface (FES) of a β-D-mannopyranose molecule associated with the ideal Stoddart conformational diagram. We have found that $^1S_5$ is among the most stable conformers and simultaneously is the most preactivated conformation in terms of elongation/shortening of the C1−O1/C1−O5 bonds, C1−O1 orientation, and charge development at the anomeric carbon. Analysis of the computed FES gives support to the proposed $^1S_5 \rightarrow B_{2,5} \rightarrow {}^OS_2$ catalytic itinerary, showing that the degree of preactivation of the substrate in glycoside hydrolases (GHs) is related to the properties of an isolated sugar ring. We introduce a simple preactivation index integrating several structural, electronic, and energetic properties that can be used to predict the conformation of the substrate in the Michaelis complex of any GH.

## 1. Introduction

Glycoside hydrolases (GHs) are the enzymes responsible for the degradation or hydrolysis of glycosidic bonds in carbohydrates. They are of greatest interest in glycobiology and glycomics,[1] as they are responsible for the modification of polysaccharides and glycoconjugates involved in numerous biological processes, such as cell−cell recognition and polysaccharide degradation for biofuel processing.[2] GHs are systematically classified into 113 families (as of July 2010) according to their sequence similarity (see http://www.cazy.org).[3] Enzymes from the same family usually share the same catalytic mechanism, in which an oxocarbenium ion-like transition state is formed.[4,5]

During the past decade, structural studies have demonstrated that GHs usually bind the substrate in a distorted conformation. For pyranoses specifically, the substrate sugar ring located at the −1 enzyme subsite distorts away from the $^4C_1$ chair conformation into a boat or skew-boat conformation (Figure 1). Experimental investigations have shown that this kind of saccharide ring distortion favors the hydrolysis reaction, and theoretical studies have demonstrated that the distorted conformation is both structurally (elongation of the leaving-group

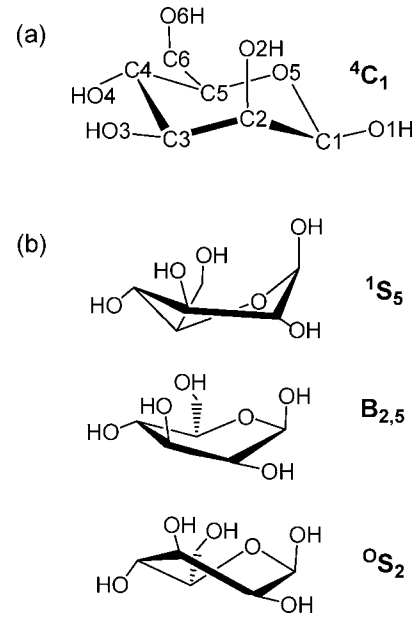


***Figure 1.*** β-D-Mannopyranose conformations: (a) the most stable gas-phase conformation; (b) conformations adopted along the catalytic itinerary in β-mannosidases.

[†] Parc Científic de Barcelona.
[‡] Universitat Ramon Llull.
[§] Institució Catalana de Recerca i Estudis Avançats.

(1) Gamblin, D. P.; Scanlan, E. M.; Davis, B. G. *Chem. Rev.* **2009**, *109*, 131–163.
(2) Pauly, M.; Keegstra, K. *Plant J.* **2008**, *54*, 559–568.
(3) Cantarel, B. L.; Coutinho, P. M.; Rancurel, C.; Bernard, T.; Lombard, V.; Henrissat, B. *Nucleic Acids Res.* **2009**, *37*, D233–D238.
(4) Rye, C. S.; Withers, S. G. *Curr. Opin. Chem. Biol.* **2000**, *4*, 573–580.
(5) Zechel, D. L.; Withers, S. G. *Acc. Chem. Res.* **2000**, *33*, 11–18.

 **10.1021/ja105520h** 

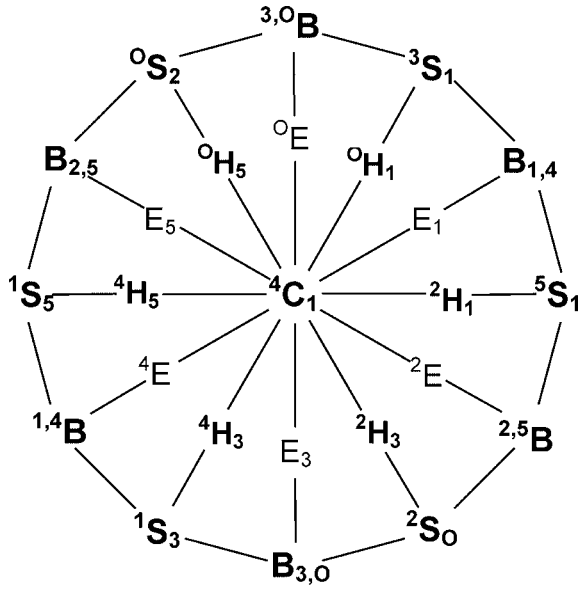


***Figure 2.*** Stoddart diagram (centered on the $^4C_1$ conformation).

distance) and electronically (charge increase at the anomeric center) similar to the oxocarbenium ion-like transition state (TS) of the GH hydrolysis reaction.[6,7] Therefore, the distorted conformation of the substrate in the Michaelis complex (MC) is "on the path" toward the TS and gives information about the *catalytic itinerary*. This is of relevant importance when designing TS-analogue-specific inhibitors for GHs, which are known to be far more potent than substrate-analogue inhibitors.[8] Catalytic itineraries of GHs are usually drawn on a Stoddart diagram (Figure 2),[9] which is a circular diagram representing all of the canonical conformations of a single pyranose ring. For instance, retaining β-D-glucosidases are known to operate via a $^4H_3$-type TS, preferentially following a $^1S_3 \rightarrow {}^4H_3 \rightarrow {}^4C_1$ itinerary, whereas α-L-fucosidases follow a $^1C_4 \rightarrow {}^3H_4 \rightarrow {}^3S_1$ itinerary.[10]

Enzymatic mannoside hydrolysis is of paramount importance for its role in the regulation of the high-mannose and complex-type glycan post-translational modifications involved in cell biology. Its malfunction can lead to a variety of diseases, including cancer.[11] This has stimulated the field of mannoside synthesis, which faces considerable challenges, mainly in the case of the β-anomers. Potential steric clashes, unsympathetic anomeric effects, and participation of the C2 neighboring group make β-anomers kinetically and thermodynamically unfavorable.[12] Therefore, parallel to smart synthetic strategies that have been applied,[13,14] mannosidase and mannosyltransferase biochemistry is blooming.[15,16]

In 2002, it was first proposed that enzymatic mannoside hydrolysis uses an unusual substrate conformational pathway.[17] For retaining β-mannosidases, structural studies of GH2 and GH26 have revealed that the β-mannosyl substrate adopts a $^1S_5$ conformation in the Michaelis complex and an $^OS_2$ conformation in the covalent intermediate of the hydrolysis reaction.[10,18] In addition, structural studies of GH5 inhibitors have suggested a $B_{2,5}$-type distortion at the TS.[19] This is further supported by a recent study by Tailford et al.[16] reporting linear free-energy relationships (LFERs) and crystal structures of TS analogues.

Detailed information concerning the energetic/structural/electronic relations of mannose is necessary for the understanding of mannosidase mechanisms and to rationalize the unfavorable effects involved in β-mannoside organic synthesis. Several theoretical studies have aimed at quantifying the relative energies of different mannopyranose ring conformations using force-field-based approaches.[20−22] It is worth mentioning the study of Dowd, French, and Reilly,[20] who computed potential energy surfaces of 16 different aldopyranose rings, including α- and β-D-mannopyranose; their work has served as a reference for subsequent studies.[23,24] Electronic rearrangements upon ring distortion, however, can be analyzed only by going beyond the force-field approximation. In recent years, a number of studies of sugar ring conformations using density functional theory (DFT) have appeared (e.g., see refs 25−32), including evaluations of

(6) Biarnés, X.; Nieto, J.; Planas, A.; Rovira, C. *J. Biol. Chem.* **2006**, *281*, 1432–1441.
(7) Soliman, M. E.; Ruggiero, G. D.; Pernia, J. J.; Greig, I. R.; Williams, I. H. *Org. Biomol. Chem.* **2009**, *7*, 460–468.
(8) Caines, M. E.; Hancock, S. M.; Tarling, C. A.; Wrodnigg, T. M.; Stick, R. V.; Stutz, A. E.; Vasella, A.; Withers, S. G.; Strynadka, N. C. *Angew. Chem., Int. Ed.* **2007**, *46*, 4474–4476.
(9) *Stereochemistry of Carbohydrates*; Stoddart, J. F., Ed.; Wiley: Toronto, 1971.
(10) Vocadlo, D. J.; Davies, G. J. *Curr. Opin. Chem. Biol.* **2008**, *12*, 539–555.
(11) Granovsky, M.; Fata, J.; Pawling, J.; Muller, W. J.; Khokha, R.; Dennis, J. W. *Nat. Med.* **2000**, *6*, 306–312.
(12) Gridley, J. J.; Osborn, H. M. I. *J. Chem. Soc., Perkin Trans.* **2000**, 1471–1491.
(13) Crich, D.; Li, L. *J. Org. Chem.* **2007**, *72*, 1681–1690.
(14) Crich, D.; Chandrasekera, N. S. *Angew. Chem., Int. Ed.* **2004**, *43*, 5386–5389.
(15) Tailford, L. E.; Ducros, V. M.; Flint, J. E.; Roberts, S. M.; Morland, C.; Zechel, D. L.; Smith, N.; Bjornvad, M. E.; Borchert, T. V.; Wilson, K. S.; Davies, G. J.; Gilbert, H. J. *Biochemistry* **2009**, *48*, 7009–7018.
(16) Tailford, L. E.; Offen, W. A.; Smith, N. L.; Dumon, C.; Morland, C.; Gratien, J.; Heck, M. P.; Stick, R. V.; Bleriot, Y.; Vasella, A.; Gilbert, H. J.; Davies, G. J. *Nat. Chem. Biol.* **2008**, *4*, 306–312.
(17) Ducros, V. M.; Zechel, D. L.; Murshudov, G. N.; Gilbert, H. J.; Szabo, L.; Stoll, D.; Withers, S. G.; Davies, G. J. *Angew. Chem., Int. Ed.* **2002**, *41*, 2824–2827.
(18) Offen, W. A.; Zechel, D. L.; Withers, S. G.; Gilbert, H. J.; Davies, G. J. *Chem. Commun.* **2009**, 2484–2486.
(19) Vincent, F.; Gloster, T. M.; Macdonald, J.; Morland, C.; Stick, R. V.; Dias, F. M.; Prates, J. A.; Fontes, C. M.; Gilbert, H. J.; Davies, G. J. *ChemBioChem* **2004**, *5*, 1596–1599.
(20) Dowd, M. K.; French, A. D.; Reilly, P. J. *Carbohydr. Res.* **1994**, *264*, 1–19.
(21) Krautler, V.; Muller, M.; Hunenberger, P. H. *Carbohydr. Res.* **2007**, *342*, 2097–2124.
(22) Barnett, C. B.; Naidoo, K. J. *Mol. Phys.* **2009**, *107*, 1243–1250.
(23) Biarnés, X.; Ardèvol, A.; Planas, A.; Rovira, C.; Laio, A.; Parrinello, M. *J. Am. Chem. Soc.* **2007**, *129*, 10686–10693.
(24) Spiwok, V.; Kralova, B.; Tvaroska, I. *Carbohydr. Res.* **2010**, *345*, 530–537.
(25) Barrows, S. E.; Dulles, F. J.; Cramer, C. J.; French, A. D.; Truhlar, D. G. *Carbohydr. Res.* **1995**, *276*, 219–251.
(26) Appell, M.; Strati, G.; Willett, J. L.; Momany, F. A. *Carbohydr. Res.* **2004**, *339*, 537–551.
(27) Schnupf, U.; Willett, J. L.; Bosma, W. B.; Momany, F. A. *Carbohydr. Res.* **2007**, *342*, 196–216.
(28) Ionescu, A. R.; Berces, A.; Zgierski, M. Z.; Whitfield, D. M.; Nukada, T. *J. Phys. Chem. A* **2005**, *109*, 8096–8105.
(29) Momany, F. A.; Appell, M.; Willett, J. L.; Schnupf, U.; Bosma, W. B. *Carbohydr. Res.* **2006**, *341*, 525–537.
(30) Appell, M.; Willett, J. L.; Momany, F. A. *Carbohydr. Res.* **2005**, *340*, 459–468.
(31) Csonka, G. I.; French, A. D.; Johnson, G. P.; Stortz, C. A. *J. Chem. Theory Comput.* **2009**, *5*, 679–692.
(32) Goerigk, L.; Grimme, S. *J. Chem. Theory Comput.* **2010**, *6*, 107–126.

different density functionals[32] and basis sets.[31] However, because of the complexity of the conformational phase space, these studies have typically been limited to a set of conformations that are stable upon geometry optimization (e.g., boats, skews, and chairs), and energy/structure/atomic charges have not been investigated in relation to experimental data for GHs.

In two previous studies,[23,33] we applied Car−Parrinello molecular dynamics (CPMD) combined with the metadynamics approach to obtain the free-energy surfaces (FESs) of $\beta$-D-glucopyranose and $\alpha$-L-fucopyranose with respect to all of the conformations in the Stoddart diagram (Figure 2).[9] It was shown that the FESs of these sugars correlate well with the conformations observed in ligand−enzyme complexes (i.e., the experimental X-ray structures of MC analogues are located in the most stable distorted minima found on the calculated FES). In this work, we have applied the same methodology to obtain the FES of $\beta$-D-mannopyranose and analyze the structural and electronic rearrangements with respect to ring conformation. In addition, we have introduced a simple index that measures the suitability of a specific conformation to be the Michaelis complex and investigate its relation to the conformations observed in the X-ray structures of E−S complexes of $\beta$-D-mannosidases.

## 2. Computational Details

**2.1. Puckering Coordinates.** Any of the possible ring conformations of a six-atom sugar ring can be unequivocally assigned using the three Cremer and Pople puckering coordinates $Q$, $\phi$, and $\theta$.[34] The $Q$ coordinate is the sum of the perpendicular distances $z_j$ of the ring atoms to the ring average plane ($Q = \sum_{j=1}^{6} z_j$). For the particular case of a pyranose ring, the $\phi$ and $\theta$ coordinates are obtained by solving the following system of equations:

$$\begin{cases} Q \sin\theta \cos\phi = \sqrt{\frac{1}{3}} \sum_{j=1}^{6} z_j \cos\left[\frac{2\pi}{6} 2(j-1)\right] \\ Q \sin\theta \sin\phi = \sqrt{\frac{1}{3}} \sum_{j=1}^{6} z_j \sin\left[\frac{2\pi}{6} 2(j-1)\right] \\ Q \cos\theta = \sqrt{\frac{1}{6}} \sum_{j=1}^{6} (-1)^{j-1} z_j \end{cases}$$

Since these are polar coordinates, any ring distortion would fall within the puckering-sphere-like volume (Figure 3). All of the possible conformations of a pyranose ring unit show variations of $Q$ (see later) that are small and fast in comparison with the variations of $\phi$ and $\theta$. Thus, the latter are the ones that differentiate between the conformers in Figure 2. At the poles ($\theta = 0$ and $\theta = \pi$) are located the two chair conformers ($^4C_1$ and $^1C_4$, respectively); in the equatorial region ($\theta = \pi/2$), the six boat and six skew structures are sequentially placed in steps of $\phi = \pi/6$.

Several representations have historically been used in order to map the three-dimensional Cremer and Pople plot onto a two-dimensional plot. The most popular are the Stoddart diagram (Figure 2), corresponding to the projection of the polar coordinates onto the equatorial plane, and the so-called plate carrée (square plane) representation, which is an equidistant cylindrical projection resulting in a rectangular map with respect to $\theta$ and $\phi$.[20] In this work, we used the former representation, which is the one commonly used in structural and mechanistic investigations of GHs.[10] Previous calculations on $\alpha$-L-fucopyranose ring using both mapping methods showed that the relative energies among the different FES minima and the most stable ring conformations computed using the metadynamics approach do not depend significantly of the type of collective variables employed (the relative free-energy differences agree within 1 kcal/mol). A small error from the dependence of the results on the DFT functional employed is also expected. Whereas atomic charges are practically independent of the DFT functional (Figure S1 in the Supporting Information), it was previously shown[23] that the relative energies might differ by $\pm$0.6 kcal/mol (on the basis of a comparison of PBE,[35] Becke-Perdew[36,37] and B3LYP[36,38]). Comparison of the CPMD/PBE/70Ry methodology used here with standard quantum chemistry approaches was performed in our previous work on $\beta$-D-glucopyranose,[23] where we showed that the relative free energy between two minima of the FES is in agreement (within 0.4 kcal/mol) with the results of previous geometry optimizations at the B3LYP/6-311++G** level of theory.

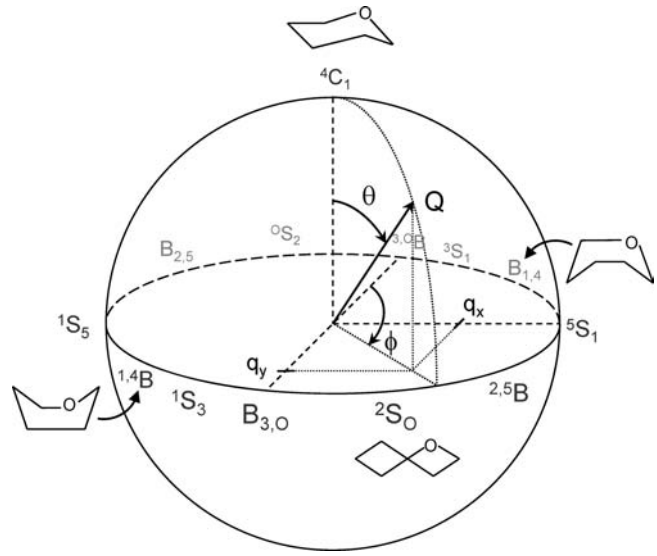


***Figure 3.*** Cremer and Pople puckering coordinates $Q$, $\theta$, and $\phi$ for a six-membered ring and the collective variables $q_x$ and $q_y$ used in the metadynamics run.

**2.2. Metadynamics Simulations.** Metadynamics is a molecular dynamics (MD)-based technique that enables the phase space to be explored and the FES to be estimated.[39] This method is based on reduction of the phase-space dimensionality to a smaller set of so-called "collective variables" (CVs) that enclose the slowest modes relevant to the process of interest. The addition of small repulsive potentials in this reduced phase space during the MD simulation enhances the exploration of the phase space. When convergence is reached, the reciprocal of the sum of the added potentials corresponds to the underlying free-energy profile in the CV space.[39] A detailed explanation of the method can be found elsewhere.[40]

To obtain the conformational FES of $\beta$-D-mannopyranose in terms of the Stoddart diagram, we used the two Cartesian

(33) Lammerts van Bueren, A.; Ardèvol, A.; Fayers-Kerr, J.; Luo, B.; Zhang, Y.; Sollogoub, M.; Blériot, Y.; Rovira, C.; Davies, G. J. *J. Am. Chem. Soc.* **2010**, *132*, 1804–1806.
(34) Cremer, D.; Pople, J. A. *J. Am. Chem. Soc.* **1975**, *97*, 1354–1358.
(35) Perdew, J. P.; Burke, K.; Ernzerhof, M. *Phys. Rev. Lett.* **1996**, *77*, 3865–3868.
(36) Becke, A. D. *Phys. Rev. A* **1988**, *38*, 3098–3100.
(37) Perdew, J. P. *Phys. Rev. B* **1986**, *33*, 8822–8824.
(38) Lee, C. T.; Yang, W. T.; Parr, R. G. *Phys. Rev. B* **1988**, *37*, 785–789.
(39) (a) Laio, A.; Parrinello, M. *Proc. Natl. Acad. Sci. U.S.A.* **2002**, *49*, 12562–12566. (b) Bussi, G.; Laio, A.; Parrinello, M. *Phys. Rev. Lett.* **2006**, *96*, 090601.
(40) Laio, A.; Gervasio, F. L. *Rep. Prog. Phys.* **2008**, *71*, 126601.

coordinates $q_x$ and $q_y$ shown in Figure 3, which are defined in terms of the Cremer and Pople puckering coordinates $Q$, $\theta$, and $\phi$ as follows:

$$q_x = Q \sin\theta \sin\phi$$

$$q_y = Q \sin\theta \cos\phi$$

These coordinates correspond to the projection of $Q$, $\theta$, and $\phi$ onto the equatorial plane and fulfill the requirements for suitable CVs in the metadynamics procedure, as described by Laio and Gervasio:[40] (i) they are explicit functions of the atomic positions and (ii) they are able to distinguish the different states of the system (i.e., all of the conformers in the Stoddart diagram). The fast variation of $Q$ ensures that the metadynamics simulation explores all possible $Q$ values for each conformer in the FES (see Figure S2 in the Supporting Information) and that their contributions to the distortion entropy are taken into account.

The two-dimensional projection ($q_x$, $q_y$) of the spherical representation of the pyranose ring conformational space ($Q$, $\theta$, $\phi$) facilitates the computation and visualization of the computed FES in a continuous space. In this way, itineraries among any three consecutive boat and skew-boat conformations can easily be drawn, as is done in structural and mechanistic studies of GHs.[10,16]

In this work, we focused on the northern hemisphere of the Cremer and Pople sphere (Figure 3) because the substrate distortions present in all of the currently available structures of MC complexes of β-mannosidases are found in this region.[10] In addition, the conformational itineraries of the mannosyl moiety during the hydrolysis reaction in either retaining or inverting β-mannosidases are expected to be limited to this region of the conformational space.

The starting structure for the simulation was the $^4C_1$ conformation. Analysis of the projection of the obtained trajectory on the puckering-sphere-like volume (data not shown) confirmed that only the northern hemisphere was sampled and that the variation of $Q$ was not limited to any particular value (Figure S2 in the Supporting Information). It should be noted that the use of the coordinates $q_x$ and $q_y$ makes it very unlikely that the system could sample more than one hemisphere, as transitions from north to south (e.g., $^4C_1$ to $^1C_4$) are not activated.

The metadynamics simulation was done within the Car−Parrinello (CP) extended Lagrangian formalism.[41] A fictitious electron mass of 850 au and a time step of 0.12 fs were used. The system temperature was set to 300 K by coupling it to a thermostat using the Nosé algorithm.[42] The simulated system consisted of a β-D-mannopyranose (24 atoms) enclosed in a orthorhombic box with dimensions 13.0 Å × 14.0 Å × 12.0 Å. The Kohn−Sham orbitals were expanded in a plane-wave (PW) basis set with a kinetic energy cutoff of 70 Ry. Ab initio pseudopotentials generated within the Troullier−Martins scheme were employed.[43] The calculations were performed using the Perdew−Burke−Ernzerhoff (PBE) generalized-gradient-corrected approximation,[35] as previously used in Car−Parrinello simulations of isolated carbohydrates and GHs.[6,23,33] About 6 ps of free dynamics was performed prior to the metadynamics simulations. Values of 10.0 amu for the mass of the fictitious particle and 0.2 au for the force constant were used in the metadynamics simulations. Gaussian-like functions with a width of 0.15 au and a height of 0.314 kcal mol$^{-1}$ were used. A Gaussian-like biasing potential was added every 12−18 fs (100−150 MD steps). A total of 13 369 Gaussians were added to reach convergence of the reconstructed FES. In terms of simulation time, this corresponded to ∼180 ps.

(41) Iannuzzi, M.; Laio, A.; Parrinello, M. *Phys. Rev. Lett.* **2003**, *90*, 238302.
(42) Nose, S. *Mol. Phys.* **1984**, *52*, 255–268.
(43) Troullier, N.; Martins, J. L. *Phys. Rev. B* **1991**, *43*, 1993–2006.

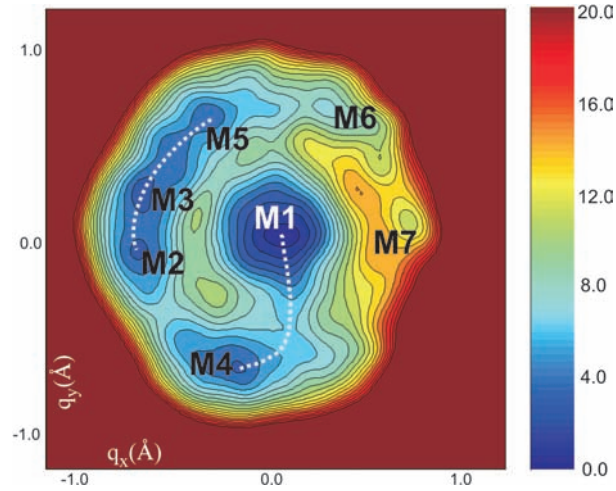


***Figure 4.*** Computed free-energy landscape of β-D-mannopyranose with respect to ring distortion. Energy values are given in kcal/mol, and each contour line of the diagram corresponds to 0.5 kcal mol$^{-1}$.

***Table 1.*** Relative Free Energies ($\Delta G_{rel}$, in kcal mol$^{-1}$) among the Main Stationary Points of the Free-Energy Surface (see Figure 3)

| minimum | conformation | $\Delta G_{rel}$ |
|---|---|---|
| M1 | $^4C_1$ | 0.0 |
| M2 | $^1S_5/^{1,4}B$ | 3.8 |
| M3 | $^1S_5/B_{2,5}$ | 3.8 |
| M4 | $^1S_3/B_{3,O}$ | 4.2 |
| M5 | $^OS_2$ | 4.8 |
| M6 | $^3S_1$ | 6.0 |
| M7 | $^5S_1$ | 6.8 |

## 3. Results and Discussion

**3.1. Conformational Free-Energy Surface.** The computed FES of β-D-mannopyranose as a function of the coordinates $q_x$ and $q_y$ (see Metadynamics Simulations) is shown in Figure 4. The corresponding representation in terms of the $\theta$ and $\phi$ puckering coordinates is provided in Figure S4 in the Supporting Information. The computed FES contains seven local minima, which are labeled as M1 to M7 according to their stability (Table 1). As expected, the most stable conformer is the undistorted $^4C_1$ chair conformation (M1). There are four minima (M2−M5) within 5 kcal mol$^{-1}$ of $^4C_1$, and the remaining ones (M6 and M7) are 6 and 7 kcal mol$^{-1}$ higher than $^4C_1$, respectively. It is also apparent from Figure 4 that among the distorted conformations (M2−M7), the most stable ones fall on the left-hand side of the diagram, whereas the right-hand side contains the highest-energy minima. Interconversion from M1 ($^4C_1$) to any of the other local minima involves energetic barriers of ≥6 kcal mol$^{-1}$, whereas some transitions around the equatorial belt might encounter barriers as low as 1 kcal mol$^{-1}$.

It was of interest to superimpose the computed free-energy landscape (Figure 4) upon the ideal representation given by the Stoddart diagram (Figure 2). To this aim, we divided the computed FES into 12 radial regions according to the $\phi$ puckering coordinate (Figure 5A). Each division line corresponds to one of the 12 different canonical conformations around the circumference of the Stoddart diagram (Figure 2). We assumed that a local minimum corresponds to a canonical conformation when its $\phi$ value is within ±7° of a division line. Intermediate conformations were assigned to minima that did not fulfill this criterion. As previously observed for other sugar rings,[23,33] not all stationary points

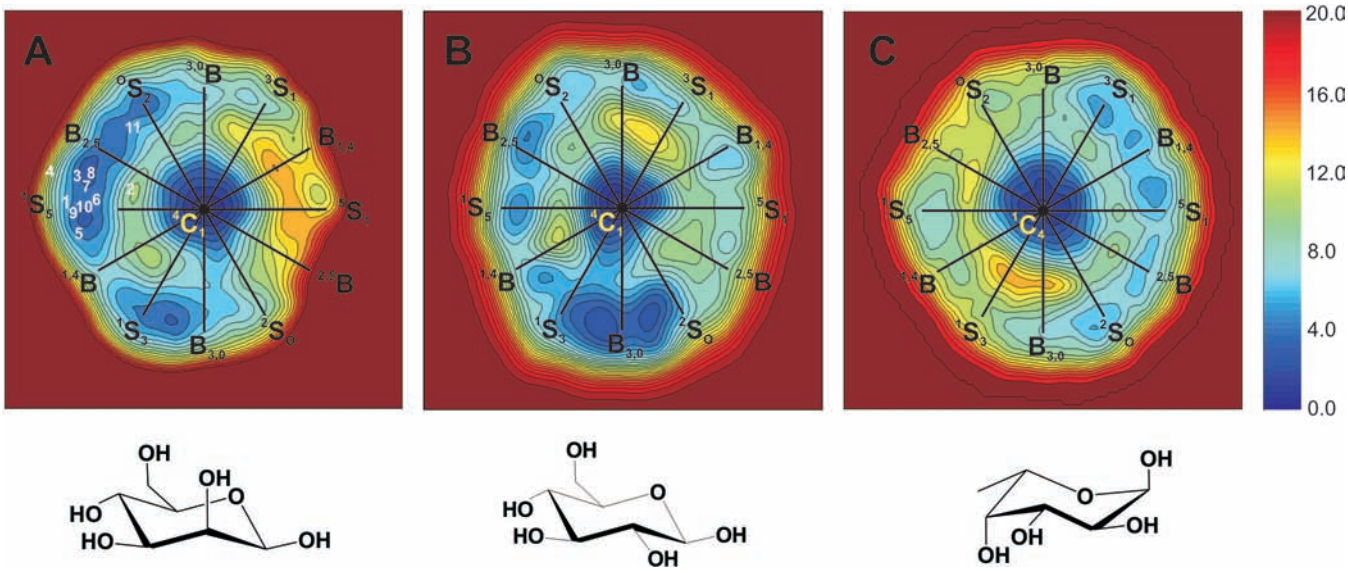


***Figure 5.*** (a) Distribution of the canonical conformations around the circumference of the Stoddart diagram (Figure 2) on the computed free-energy surface of $\beta$-D-mannopyranose. The conformations found in experimental structures of $\beta$-mannosidases are represented by numbers that correspond to the structures listed in Table 2. The results obtained for (b) $\beta$-D-glucopyranose[23] and (c) $\alpha$-L-fucopyranose[33] (southern hemisphere) are shown for comparison.

***Table 2.*** Available Complexes of $\beta$-Mannosidases and the Conformations Adopted by the Saccharide at Subsite $-$I (Also See Figure 5A)

| structure | PDB code | enzyme/ family | resolution (Å) | substrate conformation | type of structure |
|---|---|---|---|---|---|
| 1 | 2WBK[a] | $\beta$-Man2A/GH2 | 2.1 | $^{1}S_{5}$ | Michaelis complex |
| 2 | 2VJX[b] | $\beta$-Man2A/GH2 | 1.85 | $E_{5}$ | TS analogue |
| 3 | 2VL4[b] | $\beta$-Man2A/GH2 | 1.9 | $^{1}S_{5}/B_{2,5}$ | TS analogue |
| 4 | 2VO5[b] | $\beta$-Man2A/GH2 | 2.3 | $^{1}S_{5}/B_{2,5}$ | TS analogue |
| 5 | 2VR4[b] | $\beta$-Man2A/GH2 | 1.8 | $^{1}S_{5}$ | TS analogue |
| 6 | 2VQT[b] | $\beta$-Man2A/GH2 | 2.1 | $^{1}S_{5}$ | TS analogue |
| 7 | 2VOT[b] | $\beta$-Man2A/GH2 | 1.95 | $^{1}S_{5}/B_{2,5}$ | TS analogue |
| 8 | 2VMF[b] | $\beta$-Man2A/GH2 | 2.1 | $^{1}S_{5}/B_{2,5}$ | TS analogue |
| 9 | 1GVY[b] | $\beta$-Man26A/GH26 | 1.7 | $^{1}S_{5}$ | Michaelis complex |
| 10 | 1GW1[c] | $\beta$-Man26A/GH26 | 1.65 | $^{1}S_{5}$ | Michaelis complex |
| 11 | 1GW1[c] | $\beta$-Man26A/GH26 | 1.65 | $^{O}S_{2}$ | covalent intermediate |

[a] Data from ref 18. [b] Data from ref 16. [c] Data from ref 17.

of the mannose FES have a direct correspondence to the ideal conformations represented in the Stoddart diagram. For instance, M3 corresponds to a conformation between $^{1}S_{5}$ and $B_{2,5}$, while M4 lies between $^{1}S_{3}$ and $B_{3,0}$. Moreover, there are several canonical conformers (e.g., $^{2}S_{O}$, $^{2,5}B$, and $B_{1,4}$) with no direct correspondence to a computed local minimum. As a consequence, there are fewer local minima (seven) than conformations in the diagram periphery (twelve).

Comparison of the mannose FES with the ones previously computed for $\beta$-D-glucopyranose and $\alpha$-L-fucopyranose (Figure 5) reveals qualitative differences among the three energy maps. In all cases, the most stable minima lie on one side of the diagram, but this "low-energy region" shifts from northwest (mannose) to southwest (glucose) and northeast (fucose). It is noteworthy that in the case of $\alpha$-L-fucopyranose, the FES corresponds to the projection from the south pole (i.e., the central point is $^{1}C_{4}$ instead of $^{4}C_{1}$). The differences between the landscapes of mannose and glucose might seem surprising a priori, as the two rings differ only in the orientation of one hydroxyl group, 2-OH, which is equatorial in $^{4}C_{1}$-glucose but axial in $^{4}C_{1}$-mannose. Both landscapes

***Scheme 1***

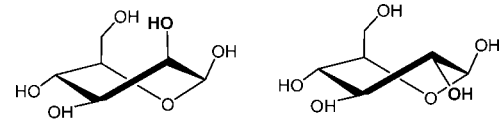


feature two stable regions, one in the $^{1,4}B-{}^{O}S_{2}$ quadrant (northwest) and the other in the $^{2}S_{O}-{}^{1,4}B$ quadrant (south). In mannose, however, the $^{2}S_{O}-{}^{1,4}B$ quadrant loses weight in favor of the $^{1,4}B-{}^{O}S_{2}$ one. This is most likely due to unfavorable interactions between the C2 exocyclic group (2-OH) and the hydroxymethyl ($CH_{2}OH$) substituent at position 5 (see Scheme 1). The $^{2}S_{O}$ conformer of mannose features an axial 2-OH group that is very close to the hydroxymethyl substituent at C5 from the $\beta$-side of the sugar ring. This leads to steric hindrance that raises the energy of $^{2}S_{O}$-mannose relative to $^{2}S_{O}$-glucose, for which the 2-OH group is equatorially oriented. Similarly, the higher energy of $^{O}S_{2}$-glucose relative to $^{O}S_{2}$-mannose is due to the steric interaction between the 2-OH group and the aliphatic hydrogen at position 5 from the $\alpha$-side of the sugar ring, an interaction that does not occur in mannose. In contrast, the $^{1}S_{3}$ distortion places the $CH_{2}OH$ substituent in a quasi-equatorial orientation, so this conformation is equally stable for both sugars.

In order to check whether there is a relation between the positions of the local minima and the occurrence of distorted conformations in enzyme-bound mannosides, we analyzed the substrate ring distortions of GH Michaelis complexes from all available $\beta$-mannosidase X-ray structures in which the sugar ring located at subsite $-$I is either a $\beta$-D-mannose derivative or a TS-analogue inhibitor (Table 2). The $q_{x}$ and $q_{y}$ coordinates of the saccharide at subsite $-$I were computed, and the corresponding value was located on the computed FES (Figure 5A). Table 2 lists the available experimental structures of $\beta$-mannoside complexes together with the conformations adopted by the substrate. Structures 1, 9, and 10 are true Michaelis complexes, whereas structures 2$-$8 correspond to complexes with TS analogues. Structure 11 (approximately $^{O}S_{2}$) corresponds to

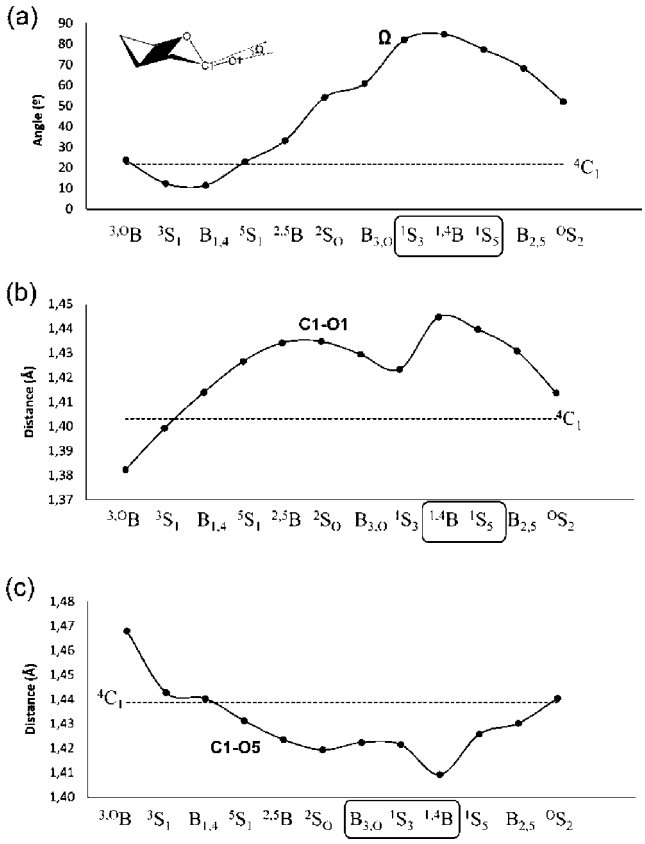


***Figure 6.*** (a) Orientation of the bond between the anomeric carbon (C1) and its exocyclic oxygen (O1), as measured by the angle Ω between the C1−O1 bond and the average plane of the ring, plotted as a function of ring conformation (see the text). (b) C1−O1 distance as a function of ring conformation. (c) Same analysis for the distance between the anomeric carbon and the ring oxygen (O5). The dotted lines represent the corresponding values obtained for the $^4C_1$ conformation using the same procedure.

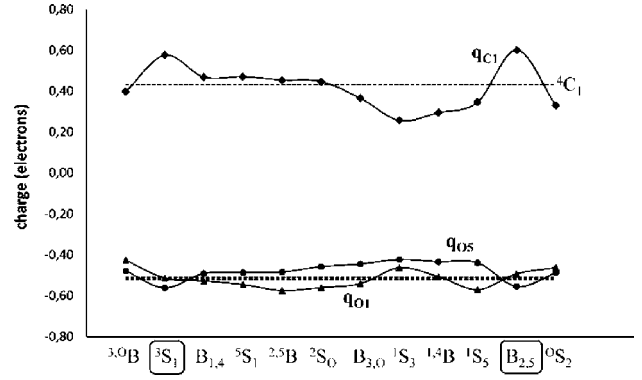


***Figure 7.*** Atomic charges on the anomeric carbon ($q_{C1}$), the ring oxygen ($q_{O5}$), and the hydroxyl oxygen of the anomeric carbon ($q_{O1}$) as functions ofring conformation. The dotted lines represent the average charges on the three atoms C1, O1, and O5 (from top to bottom) obtained for the $^4C_1$ conformation.

the covalent intermediate of the hydrolysis reaction. Interestingly, all of the experimental structures fall around one of the two most stable regions of the FES ($^1S_5$). This suggests, as previously found for β-D-glucopyranose and α-L-fucopyranose, that β-mannosidases have evolved to preferentially select those conformations of the mannosyl substrate that require less energy to be distorted.

As mentioned in the Introduction, the TS of the reaction catalyzed by GHs is known to be oxocarbenium ion-like.[4,5] Therefore, optimum catalysis relies on the condition that the C5, O5, C1, and C2 atoms are almost coplanar at the TS, favoring an $sp^2$-like hybridization of the anomeric carbon (C1) and partial double-bond formation between C1 and O5. Among all conformations of a pyranose ring, only four of them fulfill this requirement: $^4H_3/^4E$, $^3H_4/^3E$, $^{2,5}B$, and $B_{2,5}$. The two most stable distorted conformations of β-D-mannopyranose ($^1S_5$ and $^1S_3$) are next to putative TS conformers in the Stoddart diagram ($B_{2,5}$ and $^4H_3$, respectively). Interestingly, the $^OS_2$ and $^4C_1$ conformers (neighbors of $B_{2,5}$ and $^4H_3$, respectively) also correspond to local minima on the FES. Therefore, two possible reaction itineraries on the computed FES can be drawn: $^1S_5 \rightarrow B_{2,5} \rightarrow {}^OS_2$ and $^1S_3 \rightarrow {}^4H_3 \rightarrow {}^4C_1$ (Figure 4). Experimentally, however, only structures of Michaelis complexes around $^1S_5$ have been observed (Figure 5A), whereas no experimental structure around $^1S_3$ has been found. Most importantly, the experimentally observed conformation of the covalent intermediate (structure 11 in Table 2) corresponds to $^OS_2$, which determines the itinerary adopted by β-mannosidases to be $^1S_5 \rightarrow B_{2,5} \rightarrow {}^OS_2$. This suggests that factors other than the relative free energy are needed in order to understand the preferred catalytic itinerary of β-mannosidases. This will be discussed below, when an index integrating several molecular properties is defined.

**3.2. Structural and Electronic Changes.** Previous studies have found that the main changes in the substrate as it evolves from the Michaelis complex to the reaction transition state (i.e., those related to substrate preactivation) in GHs are the partial charges of C1, O1, and O5; the C1−O1 and C1−O5 bond distances; and the orientation of the C1−O1 bond (axial or equatorial).[6,7] Therefore, we focused on these parameters to analyze structural and electronic changes upon ring distortion. We selected a number of structures (240) from the metadynamics simulation that lay on the equatorial belt (our criterion was that their $\theta$ coordinate be within $\pi/8$ of the equatorial value) and submitted them to geometry optimization. The resulting structures were grouped around the canonical distortions according to their final $\phi$ values. Each of the six parameters was computed for each structure within the group, and the average values were assigned to the corresponding canonical conformation. The corresponding values for the undistorted $^4C_1$ structure were obtained from 20 optimized structures taken from a separate equilibrium simulation starting from this conformation. The potential energy profile with respect to ring distortion that was obtained from this analysis (Figure S3 in the Supporting Information) is qualitatively similar to the free-energy profile.

The orientation of the C1−O1 bond was analyzed by measuring the angle Ω between the C1−O1 bond and the average plane of the ring. As shown in Figure 6a, $^1S_3$, $^{1,4}B$, $^1S_5$, and $B_{2,5}$ display the highest Ω values (∼80°, i.e., an axial orientation of the C1−O1 glycosidic bond), whereas $^3S_1$ and $B_{1,4}$ with an equatorial C1−O1 bond have the lowest Ω (∼12°). Therefore, the most stable conformations of the FES are those featuring an axial C1−O1 bond.

The C1−O1 and C1−O5 bond distances show significant variations (0.06 Å) with ring conformation (Figure 6b,c). Distortions from $^{1,4}B$ to $B_{2,5}$ show a major increase in the C1−O1 distance and a major decrease in the C1−O5 distance. Therefore, $^{1,4}B$, $^1S_5$, and $B_{2,5}$ are the conformations that most resemble the TS of the hydrolysis reaction in terms of the C1−O1 and C1−O5 distances. Similar considerations hold for

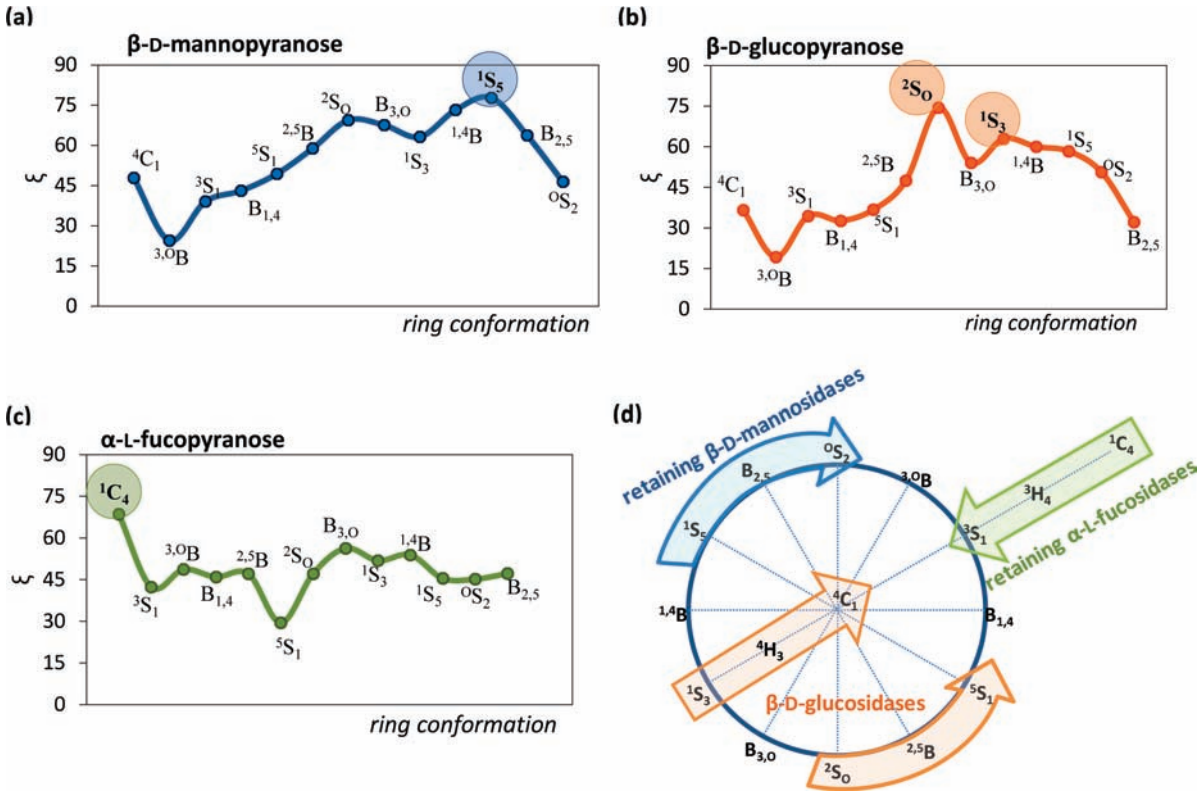


***Figure 8.*** (a−c) Variation of the values of the preactivation index $\xi$ (as defined in the text) as a function of ring conformation obtained for $\beta$-D-mannopyranose, $\beta$-D-glucopyranose, and α-L-fucopyranose. (d) Experimentally predicted catalytic conformational itineraries for retaining $\beta$-D-mannosidases (blue), $\beta$-D-glucosidases (orange), and α-L-fucosidases (green) (e.g., see ref 10).

the electronic charges (Figure 7). The conformations having a larger charge on the anomeric carbon ($q_{C1}$) are clearly $^3S_1$ and $B_{2,5}$. Therefore, the structural and electronic analysis indicate that conformations around $^1S_5$ (see Figure 5A) are preactivated for catalysis to a greater extent than those around $^1S_3$.

To complement our analysis, we combined all of the parameters analyzed above ($q_{C1}$, $q_{O5}$, $q_{O1}$, $d_{C1-O1}$, $d_{C1-O5}$, and $\Omega$) along with the relative free energy ($\Delta G_{rel}$) into a unique index that could reflect the likelihood that a given conformation would be adopted in the Michaelis complex of $\beta$-mannosidases. This was done by assigning for each conformation j a score for each parameter $x_i$ using the following formulas:

$$\text{score}(x_{i,j}) = \frac{x_{i,j} - x_{i,j}^{min}}{x_{i,j}^{max} - x_{i,j}^{min}} \times 100 \quad (x_i = d_{C1-O1}, q_{C1}, q_{O5}, \Omega)$$

$$\text{score}(x_{i,j}) = \frac{x_{i,j}^{max} - x_{i,j}}{x_{i,j}^{max} - x_{i,j}^{min}} \times 100 \quad (x_i = d_{C1-O5}, q_{O1}, \Delta G_{rel})$$

The first formula is used for those parameters for which the score increases with increasing parameter value, whereas the second is used when the score increases with decreasing parameter value. For instance, the conformation with the maximum C1−O1 distance ($^{1,4}B$, for which $d_{C1-O1} = 1.45$ Å) has the maximum $d_{C1-O1}$ score (100), whereas the minimum $d_{C1-O1}$ score (0) is assigned to $^{3,0}B$, which displays the minimum C1−O1 distance (1.33 Å). The values of the parameters and the corresponding scores are given in Table S1 in the Supporting Information. Since the score for each parameter is normalized, the scores can be directly compared, which was our main objective. We then defined an index $\xi_j$ as the average of the scores for the $n$ parameters ($n = 7$ in our case) for a given conformation j:

$$\xi_j = \frac{\sum_{i=1}^{n} \text{score}(x_{i,j})}{n}$$

In this formulation, the conformations displaying the highest values of $\xi$ are the most likely candidates to be the MC. Figure 8a shows the variation of the $\xi$ index with ring distortion. There is no single conformation with the optimum values of every parameter ($\xi = 100$). The highest values of $\xi$ occur for conformations on the left-hand side of the diagram ($B_{2,5} \rightarrow {}^2S_O$), similar to the high-energy region of the FES (Figures 4 and 5A). The conformation with the maximum $\xi$ index is $^1S_5$ ($\xi = 77.8$), whereas the value for its MC competing low-energy minimum ($^1S_3$) is significantly smaller ($\xi = 63.2$). Therefore, we conclude that $^1S_5$ is the conformation that is best prepared for catalysis in terms of energy, structure (elongation/shortening of the C1−O1/C1−O5 bonds and axiality of the C1−O1 bond), and charge development at the anomeric center. This could explain why $\beta$-mannosidases preferentially recognize the $^1S_5$ conformation and follow a $^1S_5 \rightarrow B_{2,5} \rightarrow {}^OS_2$ itinerary (Figure 8d). Similar analyses for $\beta$-D-glucopyranose and α-L-fucopyranose (Figure 8b,c) showed that the conformations with maximum $\xi$ values ($^2S_O$ and $^1S_3$ for $\beta$-D-glucopyranose and $^1C_4$ for α-L-fucopyranose) are those observed in the experimental structures of Michaelis complexes of $\beta$-D-glucosidases and α-L-fucosidases, respectively. We thus propose that the preactivation index $\xi$ can be used to predict the conformation of the substrate in the Michaelis complex of GHs.

## 4. Summary and Conclusions

By means of ab initio metadynamics simulations, we have demonstrated that the low-energy minima of the conformational free-energy surface (FES) of a free β-D-mannopyranose molecule correlate well with the observed structures of ligand−enzyme complexes and suggested that the conformations observed for Michaelis complexes of β-D-mannosidases are the ones better prepared for catalysis in terms of free energy, bond elongation/shrinking, leaving-group orientation, and charge distribution. We have shown that the computed FES can be used to predict the catalytic itinerary that the substrate follows during catalysis, giving support to the unusual $^{1}S_{5} \rightarrow B_{2,5} \rightarrow {}^{O}S_{2}$ itinerary proposed for β-D-mannosidases. We have also defined a simple index integrating several structural, electronic, and energetic properties that can be used to predict the conformation of the substrate in the Michaelis complexes of GHs.

The results obtained for mannose, together with those for glucose[23] and fucose,[33] suggest that the factors governing the distortion of the −I sugar unit in GHs are largely dictated by the intrinsic properties of a single sugar unit and that enzyme−substrate interactions may have evolved to fulfill all of the criteria required for efficient catalysis.

**Acknowledgment.** The authors thank the Spanish Ministry of Science and Innovation (MICINN) (Grant FIS2008-03845) and the Generalitat de Catalunya (GENCAT) (Grants 2009SGR-1309 and 2009SGR-82) for their financial assistance. A.A. and X.B. acknowledge an FPU Fellowship from MCINN and a Beatriu de Pinós Postdoctoral Fellowship from GENCAT, respectively. We acknowledge the computer support, technical expertise, and assistance provided by the Barcelona Supercomputing Center−Centro Nacional de Supercomputación (BSC−CNS).

**Supporting Information Available:** Values of the electronic and structural parameters defining the degree of preactivation of each mannose conformation, comparison of the atomic charges computed using B3LYP and PBE, distribution of $Q$ values for all of the conformations sampled during the metadynamics simulation, potential energy variation with respect to ring conformation, and representation of the free-energy lanscape in terms of the $\theta$ and $\phi$ puckering coordinates. This material is available free of charge via the Internet at http://pubs.acs.org.

JA105520H